Evolution of an elliptical bubble in an accelerating extensional flow

14 October 2008

Industrial Representative: J.S. Abbott (Corning, Inc.)

Faculty: C. Breward (Oxford), E. Cumberbatch (Claremont), L.J. Cummings (Nottingham), C.P. Please (Southampton), G. Richardson (Nottingham), D.W. Schwendeman (RPI), and B.S. Tilley (Olin).

Students: S. Ahmed (SUNY Buffalo), E. Fosse (Claremont), N. Gewecke (Tennessee), A. Guevara (LSU), and K. Xu (NJIT).

1 Introduction

The manufacture of optical fibers typically involves taking a solid glass cylinder (a *blank* or *preform*), heating it up to melting temperature by feeding it through a cylindrical furnace (the *drawing tower*), and drawing the molten blank from the other end of the furnace at high speed (tens of meters per second). Since the drawing speed is much faster than the feeding speed (by a factor of at least ten), along with the temperature dependence of the fiber viscosity, the molten preform stretches out, and a thin viscous fiber is formed, which rapidly cools and solidifies on exiting the drawing tower.

The basic geometry is sketched in Figure 1. The temperature of the furnace surrounding the fiber is known (prescribed) as a function of distance along the axis of the furnace, a typical temperature profile is shown in the figure. If one assumes that within the tower the fiber is sufficiently thin that its temperature is everywhere equal to the external furnace temperature, then the viscosity of the molten glass is known as a function of axial position (since the viscosity of the molten glass is known empirically as a function of temperature).

The solid preforms may contain gas bubbles, either through accident (defects in the manufactured preform) or intent (deliberate inclusion of bubbles in the preform could allow manufacture of sections of fiber with holes, which are desirable for many applications [1, 2]; as the fibre is stretched the bubble can elongate enormously). Scientists and engineers at Corning wish to gain a better understanding of how such bubbles would evolve during the draw-down process. In particular, they are interested in finding answers to the following questions:

- Given an initial bubble shape, what shape is the final bubble in the drawn fiber? For example,
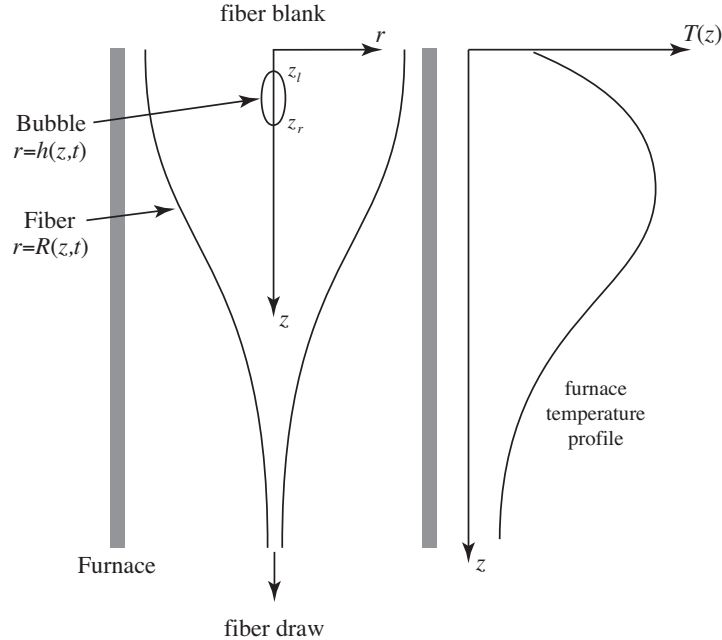
Figure 1: Schematic diagram of an optical fiber drawing process. Left: the glass blank with radius $r = R(z,t)$ and gas bubble with radius $r = h(z,t)$ for $z_\ell \leq z \leq z_r$. Right: temperature profile $T(z)$ of the furnace.

  - Is the final bubble fore-and-aft symmetric?
  - Is the final bubble the same as it would be in a fiber undergoing uniform stretching?
  - Can the bubble pinch off into two or more bubbles during its evolution?

- What factors control the final bubble shape? Contributing factors, among others, may be

  - the temperature profile of the drawing tower,
  - the viscosity of the glass,
  - the surface tension of the glass,
  - the internal pressure of the gas in the bubble,
  - the initial shape of the bubble.

- Are previous analyses of bubbles in shear flow applicable?

The fiber-drawing process outlined above is many decades old, and there is a substantial mathematical literature to which we cannot do justice in this report. What follows is therefore a highly selective overview of the historically significant papers, and recent work most pertinent to our modeling approach. Some of the earliest papers of relevance were motivated by fiber-spinning processes from the textile industry in which molten threads are extruded from a bath through an orifice (see, for example, work by Pearson and co-workers [3, 4, 5, 6]). Similar models were developed independently, or adapted from such work on textiles, for the steady drawing of optical fibers; for example [7, 8, 9]. There was other activity in this field throughout the 1970s, and Denn [10] provides a

2

useful review of this work through 1980. We also note a more recent review of extensional flows by Petrie [11], which includes very many references to fiber-drawing applications.

Systematic asymptotic models of the type that we shall use, exploiting the slenderness of the drawn fiber (its radius is much less than its length) were developed in the late 1980s and subsequently. Dewynne *et al.* [12] derived the equations governing the extensional evolution of solid isothermal viscous fibers of circular cross-section. This model was extended in [13] to include the effects of gravity and axial inertia, and provided equations for the extensional fiber velocity, the flow in the cross-section, the translation and rotation of the cross-section, and the evolution of the fiber cross-sectional area. Howell and Cummings [14, 15] extended these ideas to non-axisymmetric solid fibers, incorporating surface tension, gravity, and axial inertia to derive a model predicting the detailed cross-sectional evolution (in particular, the shape of the cross-section is predicted as a function of time) of a fiber in extensional flow. The effects of heating on an extending fiber, in particular, its impact on the viscosity, were considered by Howell *et al.* [16], who modeled the manufacture of axisymmetric glass microelectrodes (made by a similar industrial process). Wylie and Huang [17] investigated a model with both heating and axial inertia, finding that while the hotter (less viscous) regions of the fiber tend to thin and may be prone to necking and possible pinch-off, the axial inertia can be crucial in preventing pinch-off.

Drawn hollow fibers, which are more relevant to this study, were considered using similar systematic asymptotic methods by Fitt, Voyce, Monro and co-workers [1, 2, 18], and more recently by Huang *et al.* [19] and Griffiths and Howell [20, 21, 22]. Fitt *et al.* [2, 18] focussed on axisymmetric hollow fibers, taking account of variable viscosity due to the heating, and using internal hole pressurization and rotation of the input preform as process control parameters; while Huang *et al.* [19] were concerned with how the force applied to draw out the fiber can be used to control the process. The applicability of such modeling to fibers with multiple holes was considered briefly by Voyce *et al.* [18, 23]. These studies were restricted to axisymmetric geometries; however Griffiths and Howell [20, 21, 22] were concerned primarily with how to control the cross-sectional shape evolution of non-axisymmetric hollow fibers for applications such as square bottle manufacture. The proposed process control parameters here were internal hole pressurization and initial fiber cross-sectional shape.

The modeling of this report is based on that of Fitt *et al.* [1], who wrote down equations governing the evolution of an axisymmetric fiber containing a single central hole. The Navier-Stokes and heat transfer equations, with viscosity a function of temperature, are asymptotically reduced to yield a one-dimensional model in which the fiber radius, the internal hole radius, and the axial fluid velocity of the glass fiber are functions only of axial distance along the fiber, and of time t. Throughout our analysis the fiber and bubble will be assumed to remain axisymmetric; for future more comprehensive investigations we note that the evolution of slender non-axisymmetric bubbles in extensional flow was considered in work by Howell and Siegel [24], which might usefully be adapted for our problem when the assumption of axial symmetry is removed.

The remainder of the report is organized as follows. In Section 2, we describe the physical set up of the problem and corresponding mathematical model, and a reduction of the full equations is made following the work discussed in [1]. Section 3 discusses a special case of the problem in which the mass of the gas inside the bubble is fixed. This section includes a description of the governing equations of the model as well as an analysis of bubble pinch-off. The section concludes with a discussion of a numerical approach to the equations and numerical results showing the evolution of bubbles for two representative initial bubble shapes. Section 4 provides a description

of an extension of the model for the case when the gas in the bubble is allowed to diffuse into or out of the surrounding glass fiber. Governing equations of this leaky-mass model are given and a suggested numerical approach to the equations is discussed. Conclusions of the work are given in Section 5.

2 Mathematical model

A fiber is drawn in the vertical direction through a furnace whose temperature varies in the pulling direction as shown in Figure 1. The fiber is assumed to be concentric with the furnace, and the gas between the fiber and the furnace is assumed to be passive. As shown in the figure, z denote axial distance from the blank entrance region, and r is radial distance from the axis of symmetry. The two fluids, the molten glass fiber and the air surrounding it, are assumed to be immiscible, separated by an interface located at $r = R(z, t)$, where t is time. The molten glass is assumed to be a viscous, incompressible fluid whose density is independent of temperature, but whose viscosity varies significantly with temperature. A third region, defined by $r \leq h(z, t)$ for $z_\ell(t) \leq z \leq z_r(t)$, contains a gas bubble. The gas is assumed to be ideal and compressible. Further, it is assumed that the pressure of the gas in the bubble is spatially uniform since the time scale associated with acoustic signals is much shorter than the time it takes for the bubble to be advected with the surrounding glass through the drawing tower. In what follows, we assume that the temperature, $T(z)$, is a known quantity throughout the regions of interest, and that energy is automatically conserved.

From these assumptions, the glass region is governed by continuity and conservation of momentum, i.e.

$$\nabla \cdot \mathbf{u} = 0, \tag{1}$$

$$\rho_0 \frac{D\mathbf{u}}{Dt} = \nabla \cdot \tau + \rho_0 g \mathbf{e}_z, \tag{2}$$

where $\mathbf{u}$ is the velocity of the glass, ρ_0 is the glass density, τ is the stress tensor, g is the acceleration due to gravity, and $\mathbf{e}_z$ is the unit vector in the axial direction. The stress tensor is given by

$$\tau = -p\mathbf{I} + \mu(T)\left(\nabla\mathbf{u} + \nabla\mathbf{u}^T\right), \tag{3}$$

where p is pressure, $\mathbf{I}$ is the identity tensor, and $\mu(T)$ is the temperature-dependent viscosity of the molton glass. For the gas bubble, we assume that its density ρ_g and pressure P_g obey the ideal gas law

$$P_g = \rho_g R_m T, \tag{4}$$

where R_m is the mass-based universal gas constant. Further equations for the gas depend on whether the mass in the bubble is assumed to be fixed or not. These equations will be discussed later in Sections 3 and 4 for the *fixed-mass* and *leaky-mass* models, respectively.

Equations at the interfaces between the bubble and the glass and between the glass and the surrounding air are needed to complete the description. At the interface, $r = h(z, t)$, between the bubble and the glass we assume that tangential component of stress is continuous and that the normal component of stress is balanced by capillary forces, i.e.

$$\mathbf{t}_1 \cdot \tau \cdot \mathbf{n}_1 = 0, \tag{5}$$

$$\mathbf{n}_1 \cdot \tau \cdot \mathbf{n}_1 = -P_g + \gamma\kappa, \tag{6}$$

4

where $\mathbf{t}_1$ and $\mathbf{n}_1$ denote the tangential and normal components of the surface of the bubble, respectively, γ is the surface tension between the gas in the bubble and the surrounding glass, and κ is the curvature of the free surface of the bubble. (Generally, surface tension is function of temperature T, but we take it to be constant for simplicity.) Similar condition apply at the interface, $r = R(z,t)$, between the glass and the ambient gas outside the fiber, namely,

$$\mathbf{t}_2 \cdot \tau \cdot \mathbf{n}_2 = 0, \tag{7}$$

$$\mathbf{n}_2 \cdot \tau \cdot \mathbf{n}_2 = -P_a + \gamma_a \kappa_a, \tag{8}$$

where $\mathbf{t}_2$ and $\mathbf{n}_2$ denote the tangential and normal components of the surface of the glass fiber, respectively, P_a is the ambient pressure of the gas outside of the fiber, γ_a is the surface tension between the glass and the ambient gas surrounding it, and κ_a is the curvature of the free surface of the glass fiber. We assume that P_a does not depend significantly on temperature, and thus take it to be constant.

Quantity	Range
axial length	1 m
glass radius	$10^{-1} - 10^{-4}$ m
bubble radius	$10^{-5} - 10^{-8}$ m
glass viscosity	$10^5 - 10^6$ Pa s
axial velocity	$10^{-3} - 10^1$ m s^{-1}

Table 1: Ranges for various dimensional quantities of the system.

Ranges for various quantities of the system are listed in Table 1. The axial length of the system is determined by the length of the drawing tower which is approximately one meter, while the thickness of the fiber varies from centimeters as the glass blank enters the tower to hundreds of microns at the end of the fiber draw. This observation suggests that a thin-layer approach can be used to reduce the full system of equations to a simpler set of coupled equations. This reduction has been used in a number of previous papers. In particular, Fitt *et al.* [1] employ this approach for an axisymmetric fiber with a co-axial gas hole. They assume that the radius of the fiber and the hole are of similar order, and arrive at the following reduced equations

$$\rho_0 \left(R^2 - h^2 \right) \left(w_t + w w_z - g \right) = \left[3\mu \left(R^2 - h^2 \right) w_z + \gamma \left(R + h \right) \right]_z, \tag{9}$$

$$\left(h^2 \right)_t + \left(h^2 w \right)_z = \frac{\left(P_g - P_a \right) R^2 h^2 - \gamma R h \left(R + h \right)}{\mu \left(R^2 - h^2 \right)}, \tag{10}$$

$$\left(R^2 \right)_t + \left(R^2 w \right)_z = \frac{\left(P_g - P_a \right) R^2 h^2 - \gamma R h \left(R + h \right)}{\mu \left(R^2 - h^2 \right)}, \tag{11}$$

where w is the axial component of velocity in the glass fiber. These equations may be employed for the present problem by treating the gas hole as our gas bubble. We then make a further reduction based on the observation that the radius of the gas bubble is much smaller than the radius of the glass fiber, and these equations form the building blocks of the fixed-mass and leaky-mass models considered in the next two sections.

5

3 Fixed-mass model

In this section, we consider a model for the behavior of a bubble in which the mass of gas inside the bubble is assumed to be fixed with time. We begin by discussing the governing equations for the model, and then perform an analysis of pinch-off. The section ends with a discussion of a numerical treatment of the equations and results for two different initial bubble configurations.

3.1 Governing equations

The governing equations for the model may be obtained from (9), (10) and (11) in the following manner. For the glass, we subtract (10) from (11) to obtain

$$\left(R^2 - h^2\right)_t + \left((R^2 - h^2)w\right)_z = 0.$$

Assuming that the flow of molten glass is steady and that $h \ll R$ gives

$$(Aw)_z = 0, \tag{12}$$

where $A(z) = R^2$ is the "area" of the glass fiber. Applying the same two assumptions to (9) gives

$$\rho_0 A \left(ww_z - g\right) = \left[3\mu A w_z + \gamma\sqrt{A}\right]_z.$$

A further assumption that the Reynolds number is small gives

$$-\rho_0 g A = \left[3\mu A w_z + \gamma\sqrt{A}\right]_z. \tag{13}$$

The steady equations in (12) and (13) for the glass are considered for the interval $z \geq z_0$ with boundary conditions taken to be

$$A = A_0, \quad w = w_0 \quad \text{at } z = z_0 \qquad \text{and} \qquad A = A_\infty \quad \text{as } z \to \infty.$$

It is clear from (12) and the boundary conditions that

$$Aw = A_0 w_0,$$

and this may be used to eliminate A or w in (13) which is done later.

A gas bubble is assumed to exist on the interval $z_\ell(t) \leq z \leq z_r(t)$ and have radius given by $h(z,t)$ as discussed previously and shown in Figure 1. The two ends of the bubble advect with the flow of glass so that

$$\frac{d}{dt} z_k(t) = w(z_k(t)), \qquad k = \ell \text{ or } r.$$

An equation for the radius of the bubble may be obtained from (10). As before, we assume $h \ll R$ which gives

$$q_t + (wq)_z = \frac{1}{\mu} \left(Pq - \gamma\sqrt{q}\right), \tag{14}$$

where $q(z,t) = h^2$ is the "area" of the bubble and $P = P_g - P_a$ is the "gauge" pressure of the gas in the bubble. The assumption of fixed mass implies

$$\int_{\mathcal{V}_b} \rho_g \, dV = \int_{\mathcal{V}_b} \frac{P_g}{R_m T} \, dV = \mathcal{M}_g,$$

6

where $\mathcal{V}_b$ is the volume of the bubble and $\mathcal{M}_g$ is the mass of the gas in the bubble. In terms of the geometry of the bubble and using the assumption that the gas pressure is spatially uniform gives

$$(P(t) + P_a) \int_{z_\ell(t)}^{z_r(t)} \frac{q(z,t)}{T(z)} \, dz = M, \tag{15}$$

where $M = R_m \mathcal{M}_g / \pi$. It is assumed that z_ℓ and z_r are known at $t = 0$, with $z_0 \leq z_\ell(0) < z_r(0)$, and that

$$q(z,0) = \begin{cases} q_0(z), & \text{for } z_\ell(0) \leq z \leq z_r(0), \\ 0, & \text{otherwise,} \end{cases}$$

where $q_0(z)$ specifies the initial shape of the bubble. The boundary condition is $q(z_0, t) = 0$, and $P(0)$ is assumed to be known so that M is given by

$$M = (P(0) + P_a) \int_{z_\ell(0)}^{z_r(0)} \frac{q_0(z)}{T(z)} \, dz.$$

For later purposes, we find it convenient to introduce an area-weighted coordinate

$$x = \int_{z_0}^{z} \frac{A(\zeta)}{A_0} \, d\zeta, \qquad \text{so that} \qquad \frac{dx}{dz} = \frac{A}{A_0} = \frac{w_0}{w}.$$

In terms of the new variable x, (13) becomes

$$-\rho_0 g A_0 = \left[-3 w_0 \mu A_x + \gamma \sqrt{A} \right]_x, \tag{16}$$

which may be integrated once to give

$$A_x = -\frac{K - \rho_0 g A_0 x - \gamma \sqrt{A}}{3 w_0 \mu (T(z))}, \qquad x \geq 0, \tag{17}$$

where $K > 0$ is a constant of integration. Equation (17) together with

$$z_x = \frac{A_0}{A}, \qquad x \geq 0, \tag{18}$$

may be solved numerically subject to the conditions $z(0) = z_0$, $A(0) = A_0$ and $\lim_{x \to \infty} = A_\infty$ to determine $z(x)$, $A(x)$ and K. The axial velocity of the glass fiber is then given by

$$w(x) = \frac{w_0 A_0}{A(x)}.$$

In terms of the variables (x, t), the bubble equations in (14) and (15) become

$$y_t + w_0 y_x = \frac{1}{\mu} \left(Py - \gamma \sqrt{wy} \right), \tag{19}$$

$$(P(t) + P_a) \int_{x_\ell(t)}^{x_r(t)} \frac{y(x,t)}{T(z(x))} \, dx = \tilde{M}, \tag{20}$$

where $y(x,t) = wq$, $\mu = \mu(T(z(x)))$ and $\tilde{M} = w_0 M$. The positions of the left and right ends of the bubble are $x_k(t) = x_k(0) + w_0 t$, $k = \ell$ or r, where $z(x_k(0)) = z_k(0)$. The equation in (19) for $y(x,t)$ is hyperbolic and may be solved along characteristics $x - w_0 t = $ constant which are now straight lines.

In view of the differential operator on the left-hand-side of (19), it is convenient to switch to (ξ, t), where $\xi = x - w_0 t$, to get

$$y_t = \frac{1}{\mu}\left(Py - \gamma\sqrt{wy}\right), \qquad \xi_\ell < \xi < \xi_r, \quad t > 0, \tag{21}$$

$$(P(t) + P_a)\int_{\xi_\ell}^{\xi_r} \frac{y(\xi,t)}{T(z(\xi + w_0 t))}\, d\xi = \tilde{M}, \qquad t > 0, \tag{22}$$

where $w = w_0 A_0 / A(\xi + w_0 t)$ and $\mu = \mu(T(z(\xi + w_0 t)))$. The variable ξ essentially marks the particular characteristic on which (21) is to be integrated in time t. The form of the equations in (21) and (22) is particularly convenient for a numerical integration as is discussed in Section 3.3.

3.2 Pinch-off analysis

One of the questions of interest to researchers at Corning is whether the bubble evolves as a single entity with rounded ends, or whether "pinch-off" can occur, acting either to "zip up" the bubble from its ends, or to close the bubble at an interior point for bubbles of non-convex initial shape, giving rise to two (or more) disconnected bubbles. In order to understand the process by which such pinch-off might occur we perform an analysis of two simple local models.

3.2.1 Constant-coefficient model

The behavior of the bubble radius is governed by (21), where $y = wh^2$, with the pressure determined by (22). In view of the right-hand-side of (21), it is clear that the first term involving pressure acts to increase the bubble radius while the second term involving surface tension acts to decrease it. These two terms are in competition, and if the second one wins, then the bubble may pinch-off. To model this behavior approximately, a simple approach is to treat the coefficients in the equation as constant so that (22) decouples and (21) may be solved exactly. In this approach, (21) becomes

$$y_t = Ay - B\sqrt{y}, \qquad y(t_0) = y_0, \tag{23}$$

where

$$A = \frac{P}{\mu}, \qquad B = \frac{\gamma\sqrt{w}}{\mu},$$

are assumed to be known positive constants, and y_0 is some known value of y at a time $t = t_0$. A straightforward analysis of (23) shows that if $\sqrt{y_0} > B/A = \gamma\sqrt{w}/P$, then the solution grows in time, whereas if $\sqrt{y_0} < \gamma\sqrt{w}/P$, then the solution decreases and ultimately pinches off when $y = 0$ and thus $h = 0$. Since $y = wh^2$, the condition for pinch-off is simply

$$h_0 < \gamma/P,$$

and pinch-off occurs at

$$t = t_0 + \frac{2\mu}{P}\ln\left(\frac{\gamma/P}{\gamma/P - h_0}\right).$$

8

3.2.2 Vanishing-radius model

A second approach is to perform a straightforward local analysis of the equations as $h \to 0$. At leading order (14) takes the form

$$h_t + wh_z = -\frac{\gamma}{2\mu}, \tag{24}$$

hence $h = -\gamma t/(2\mu) + H$, where H satisfies the hyperbolic PDE

$$H_t + wH_z = 0.$$

Thus, H is constant along characteristics $dz/dt = w$ moving with the axial velocity, so that for a material point of the glass-bubble interface with initial bubble radius h_0, the radius at subsequent times t satisfies

$$h = h_0 - \frac{\gamma t}{2\mu} \quad \text{along characteristics} \quad \frac{dz}{dt} = w.$$

In the absence of surface tension, $\gamma = 0$, the bubble would simply be stretched out by the extensional flow, with the end points where $h = 0$ being advected by the flow with speed w. The above shows that surface tension acts to make the bubble shorter than this, so that in Lagrangian coordinates traveling with the flow the bubble retracts from its ends. If Z denotes the initial position of the point $z(t)$ traveling with the flow, such that

$$\frac{dz}{dt} = w(z), \quad \text{with } z(0) = Z,$$

then (at points where h is small, so that our approximate analysis applies) the bubble radius $h(z(t), t)$ satisfies

$$h(z(t), t) = h_0(Z) - \frac{\gamma t}{2\mu}.$$

Thus, if the right-hand end of the bubble is initially marked by point Z_0, with $h_0(Z_0) = 0$, and if $Z_1 < Z_0$ is some initial point within the bubble support, with $h_0(Z_1) = h_1 > 0$, then the bubble will pinch-off to the material point in the flow marked by Z_1 at time $t_1 = 2\mu h_1/\gamma$. This is indicated in Figure 2.

3.3 Numerical method and results

A numerical treatment of the governing equations for the glass fiber and for the gas bubble proceeds in two steps. In the first step, the equations in (17) and (18) are solved to determine the behavior of the fiber. This result then provides input for the numerical integration of equations (21) and (22) to determine the behavior of the bubble in the second step.

For the first step, we require a temperature profile. We use

$$T(z) = \begin{cases} T_0(z) & \text{for } z_0 \leq z \leq z_1, \\ T_0(z)\left(\dfrac{z_2 - z}{z_2 - z_1}\right) + T_1(z)\left(\dfrac{z - z_1}{z_2 - z_1}\right) & \text{for } z_1 < z < z_2, \\ T_1(z) & \text{for } z \geq z_2, \end{cases} \tag{25}$$

where

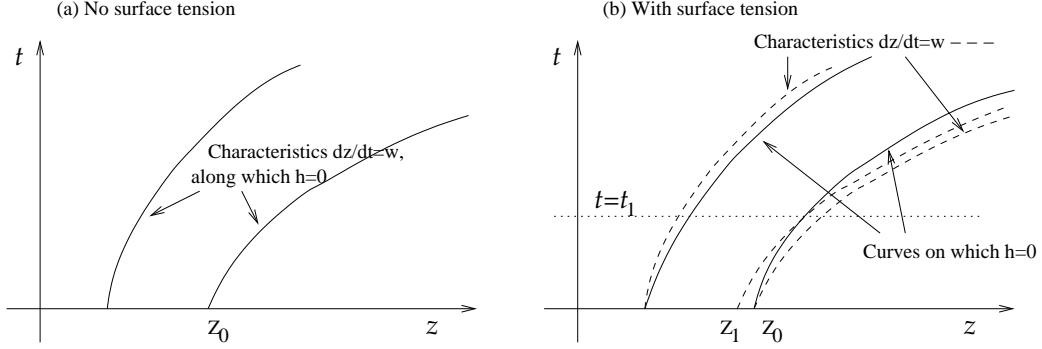$$z_0 = 0.4 \text{ m}, \qquad z_1 = 0.9 \text{ m}, \qquad z_2 = 1.2 \text{ m}.$$

Figure 2: Sketch showing the characteristic curves of the model equation in (24), together with the curves on which $h = 0$ for a typical extensional flow. Case (a) indicates that for $\gamma = 0$ the curves on which $h = 0$ coincide with characteristics and are simply advected with the flow. Case (b) shows that curves on which $h = 0$ may cross characteristics leading to the bubble being shorter than would be expected due to pure advective stretching.

The temperature profile given by $T_0(z)$ is a polynomial fit to artificial "model" data constructed by Corning for the workshop. It is given in degrees Kelvin by

$$T_0(z) = 273 + 2200 \sum_{n=0}^{8} a_n z^n,$$

where z is given in meters, and

$$a_0 = 0.6335, \qquad a_1 = 0.2856, \qquad a_2 = 8.9977, \qquad a_3 = -38.5190, \qquad a_4 = 68.9370,$$

$$a_5 = -62.6802, \qquad a_6 = 26.6232, \qquad a_7 = -2.6393, \qquad a_8 = -0.8689.$$

The temperature profile given by $T_1(z)$ provides an exponential decay to an ambient temperature, and is given by

$$T_1(z) = 273 + d_0 \exp(-d_1 z), \qquad d_0 = 3687.1, \qquad d_1 = 0.7833.$$

In addition to an assumed temperature profile, we require a formula for the viscosity of molten glass as a function of temperature. As suggested by Corning for workshop purposes, we use the artificial formula

$$\mu(T) = \frac{1}{10} \exp\left(b_0 + \frac{b_1}{T}\right), \qquad b_0 = -9.81, \qquad b_1 = 55038. \tag{26}$$

Here T is given in degrees Kelvin and μ is given in pascal-seconds. (All quantities in this report are taken in SI units unless noted otherwise.) Figure 3 shows the temperature profile given by (25) on the left and the corresponding behavior of the viscosity on the right.

Having specified a temperature profile and formula for the viscosity, we are now in a position to integrate (17) and (18) numerically to determine $A(z)$ and $w(z)$ for the glass fiber. The initial conditions for these ODEs at $x = 0$ are taken to be

$$z(0) = z_0 = 0.4 \text{ m}, \qquad A(0) = A_0 = 1.296 \times 10^{-5} \text{ m}^2 \quad (R_0 = 3.6 \text{ mm}),$$
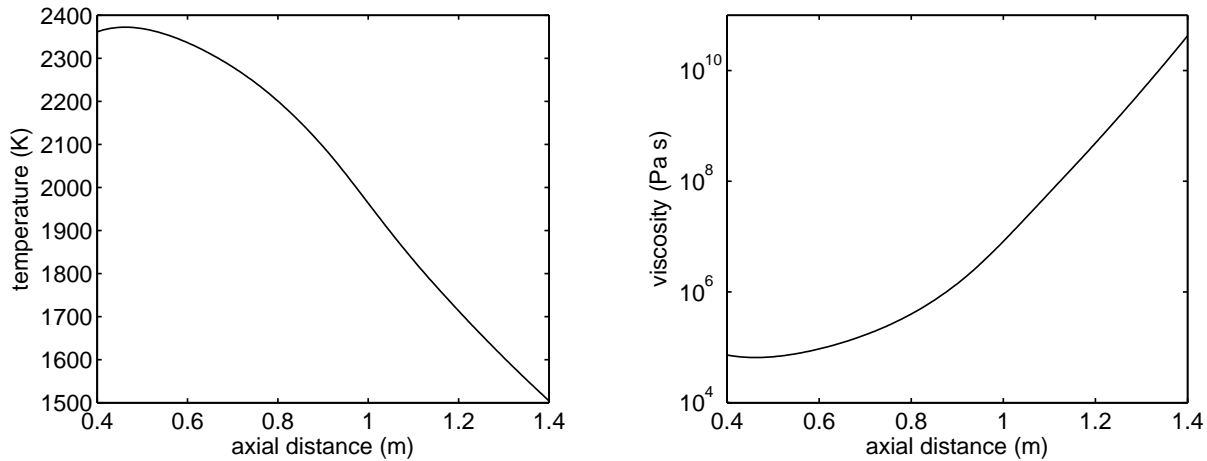
10

Figure 3: Temperature profile $T(z)$ and corresponding viscosity $\mu(T(z))$.

and the remaining parameters in the equations are

$$\rho_0 = 2.2 \times 10^3 \text{ kg/m}^3, \qquad P_a = 101325 \text{ Pa},$$

$$g = 9.8 \text{ m/s}^2, \qquad \gamma = 0.28 \text{ N/m}, \qquad w_0 = 0.003 \text{ m/s}.$$

A provisional choice for the constant K in (17) is made and the two ODEs are integrated numerically using a second-order Runge-Kutta method for $0 \le x \le x_\infty$, where $x_\infty = 0.0359$ (which corresponds to $z_\infty \approx 1$ m). The value for K is adjusted until

$$A(x_\infty) = A_\infty = 3.9062 \times 10^{-9} \text{ m}^2 \quad (R_\infty = 0.0625 \text{ mm}).$$

It is found that $K = 0.225036503$, and plots for $R = \sqrt{A}$ and w versus z are shown in Figure 4. In the plots, we include artificial model data provided by Corning, which we also list in Table 2. We note that the curves given by a numerical integration of the equations and the marks given by the model data are in good agreement (i.e., the numerical integration generating the artificial data agrees with the current model, as it should). It should also be noted that the contribution of gravity in (17) was found to play a negligible role, and thus the term could have been left out without significant loss of accuracy.

The second step of the numerical scheme involves an integration of the equations in (21) and (22) for the bubble. The interval $[\xi_\ell, \xi_r]$ is represented by a uniform grid, $\xi_j = \xi_\ell + j\Delta\xi$, $j = 0, 1, \ldots, N$, where $\Delta\xi = (\xi_r - \xi_\ell)/N$. We define y_j^n to be an approximation for y at ξ_j and at a time $t_n = n\Delta t$, where $\Delta\xi = w_0\Delta t$ so that the characteristics are aligned with the grid in space-time. Likewise, we define P^n to be an approximation for P at t_n. From the integration of the equations for the glass fiber, we assume that $z(x)$, $w(x)$ and $A(x)$ are known, and thus $T(z(x))$ and $\mu(T(z(x)))$ are known as well. Initially, we set

$$y_j^0 = w(\xi_j)q_0(z(\xi_j)), \qquad P^0 = \frac{\gamma \sum_j \sqrt{q_0(z(\xi_j))}}{\sum_j q_0(z(\xi_j))}.$$

The former condition specifies the initial shape of the bubble while the latter condition assumes the initial pressure is determined by an average balance of pressure and surface tension for the bubble.
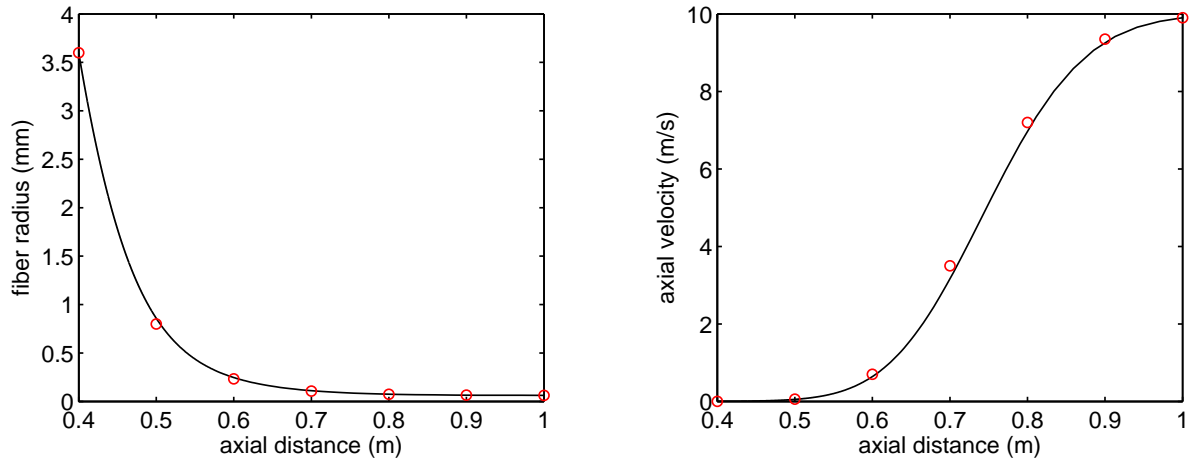
11

Figure 4: Outer radius $R = \sqrt{A}$ and axial velocity w versus z. Solid curves are from a numerical integration and marks are from data provided by Corning.

z (m)	$R = \sqrt{A}$ (mm)	w (m/s)
0.4	3.600	0.003
0.5	0.8000	0.060
0.6	0.2325	0.700
0.7	0.1070	3.50
0.8	0.07350	7.20
0.9	0.06465	9.35
1.0	0.06280	9.90

Table 2: Data for outer radius $R = \sqrt{A}$ and axial velocity w versus z.

As with the integration of the equations for the glass fiber, we choose an explicit, second-order, Runge-Kutta-type scheme involving a two-stage, midpoint-type procedure. In the first stage, assuming that y_j^n and P^n are known, we compute y_j^* and P^* from the equations

$$y_j^* = y_j^n + \frac{\Delta t}{2\mu_{j+n}} \left(P^n y_j^n - \gamma \sqrt{w_{j+n} y_j^n} \right), \qquad j = 0, 1, \ldots, N,$$

$$(P^* + P_a) \sum_{j=1}^{N} \left(\frac{y_{j-1}^*}{T_{j+n-1/2}} + \frac{y_j^*}{T_{j+n+1/2}} \right) \frac{\Delta\xi}{2} = \tilde{M},$$

where w_k, T_k and μ_k are defined by $w(k\Delta\xi)$, $T(z(k\Delta\xi))$ and $\mu(T_k)$, respectively. The mass constant, $\tilde{M}$, is determined initially by

$$\tilde{M} = \left(P^0 + P_a \right) \sum_{j=1}^{N} \left(\frac{y_{j-1}^0}{T_{j-1}} + \frac{y_j^0}{T_j} \right) \frac{\Delta\xi}{2}.$$

In the second stage, we compute y_j^{n+1} and P^{n+1} from the equations

$$y_j^{n+1} = y_j^n + \frac{\Delta t}{\mu_{j+n+1/2}} \left(P^* y_j^* - \gamma \sqrt{w_{j+n+1/2} y_j^*} \right), \qquad j = 0, 1, \ldots, N,$$

$$\left(P^{n+1} + P_a \right) \sum_{j=1}^{N} \left(\frac{y_{j-1}^{n+1}}{T_{j+n}} + \frac{y_j^{n+1}}{T_{j+n+1}} \right) \frac{\Delta\xi}{2} = \tilde{M}.$$

The first stage represents a forward-Euler half-step, while the second stage provides the second-order correction.

It should be noted that if y_j^n becomes negative for some $j = J$ say, then we assume that the bubble has pinched off at that location and set $y_J^n = 0$. If the pinch-off occurs on either end of the bubble, then there is no essential difficulty with the calculation of pressure for the remainder of the evolution. If, on the other hand, the pinch-off occurs in the interior of the bubble, as it might for a non-convex bubble shape (see Section 3.3.2), then a separate uniform pressure is computed for each part of the bubble on either side of the pinch-off. The formulas above still apply, but for a restricted range of j, e.g., $j = 0, 1, \ldots, J$ for the left-part of the bubble and $j = J, J+1, \ldots, N$ for the right-part of the bubble.

3.3.1   Example: convex bubble

Let us first consider an example in which the initial bubble shape is convex. We take

$$q_0(z) = 4h_{\max}^2 \zeta(1 - \zeta), \qquad \zeta = \frac{z - z_\ell(0)}{z_r(0) - z_\ell(0)},$$

where

$$h_{\max} = 5 \times 10^{-7} \text{ m}, \qquad z_\ell(0) = .4 \text{ m}, \qquad z_r(0) = .4001 \text{ m},$$

which corresponds to a bubble in the shape of an ellipsoid with a length equal to 100 μm and a maximum radius equal to 0.1 μm. The initial pressure for this bubble shape is $P^0 = 659.5$ kPa.

For this calculation, we use $N = 200$ and integrate the equations for the bubble until the left end of the bubble has passed $z = 1.1$ m.

The plots in Figure 5(a–h) show the evolution of the bubble from its initial shape. As the glass accelerates through the drawdown process, the bubble is stretched and elongates. The ratio of the bubble radius to its axial length is 10^{-3} initially, but this ratio decreases dramatically by the end of the fiber draw. For this initial shape, the bubble elongates to an axial distance of 0.3180 m and a maximum radius of 7.767×10^{-9} m by the end of the draw, so that the ratio decreases to 2.443×10^{-8}. The initial shape has fore-aft symmetry, but loses this symmetry during the elongation. However, once the drawdown is complete, fore-aft appears to be recovered. It is also noted that the ends of the bubbles shown in the figure have pinched off slightly, even as early as the plot shown in Figure 5(b). The amount of bubble pinch-off increases very slowly during the evolution.

Figure 6(a) shows the behavior of the bubble pressure. The color of the marks in the figure correspond to the eight bubble shapes shown in Figure 5. As the bubble elongates, the pressure increases due to the initial decrease in the volume of the bubble. (Recall that the mass of the gas in the bubble is assumed to be fixed.) Later during the evolution, the pressure decreases which is due to the effect of the decrease in temperature of the glass surrounding the bubble. In Figure 6(b), we provide a quantitative measure of fore-aft symmetry of the bubble. At each time t, we compute

$$\Delta h(t) = \left\{ \frac{\int_{z_\ell}^{z_m} (h(z,t) - h(z_r - z, t))^2 \, dz}{\int_{z_\ell}^{z_m} h(z,t)^2 \, dz} \right\}^{1/2}, \qquad z_m(t) = \frac{1}{2} (z_\ell(t) + z_r(t)),$$

which measures the L_2 deviation from symmetry about the midpoint, z_m, of the bubble. A bubble with fore-aft symmetry has $\Delta h = 0$, while $\Delta h > 0$ for a bubble without symmetry. The plot in the figure shows $\Delta h(t)$ versus $z_\ell(t)$ and confirms that the bubble is symmetric initially, loses the symmetry during the elongation, but then regains this symmetry (within numerical approximation) by the end of the fiber draw.

3.3.2 Example: non-convex bubble

As a second example, we consider the case of a non-convex initial bubble shape. We set

$$q_0(z) = h_{\min}^2 + Q_1 \hat\zeta^2 + Q_2 \hat\zeta^4, \qquad \hat\zeta = \frac{2z - z_\ell(0) - z_r(0)}{z_r(0) - z_\ell(0)}, \tag{27}$$

where

$$Q_1 = 2(h_{\max}^2 - h_{\min}^2) + 2h_{\max}\sqrt{h_{\max}^2 - h_{\min}^2}, \qquad Q_2 = -h_{\min}^2 - Q_1.$$

The shape given by (27) resembles a dumbbell. It has fore-aft symmetry about $z_m(0) = (z_\ell(0) + z_r(0))/2$ with a minimum radius given by $h_{\min}$ at $z = z_m$ and a maximum radius given by $h_{\max}$ at two points on either size of the midpoint. We use the same values for $h_{\max}$, $z_\ell(0)$ and $z_r(0)$ as in the previous example in addition to setting $h_{\min} = h_{\max}/5$. The initial pressure for this bubble shape is $P^0 = 705.1$ kPa, and we use $N = 200$ as before.

The plots in Figure 7(a–h) show the evolution of the bubble from its initial non-convex shape. For this case, pinch-off occurs relatively soon during the fiber draw so that the bubble evolves into two separate bubbles, each with its own uniform pressure. As before, the bubble elongates severely.
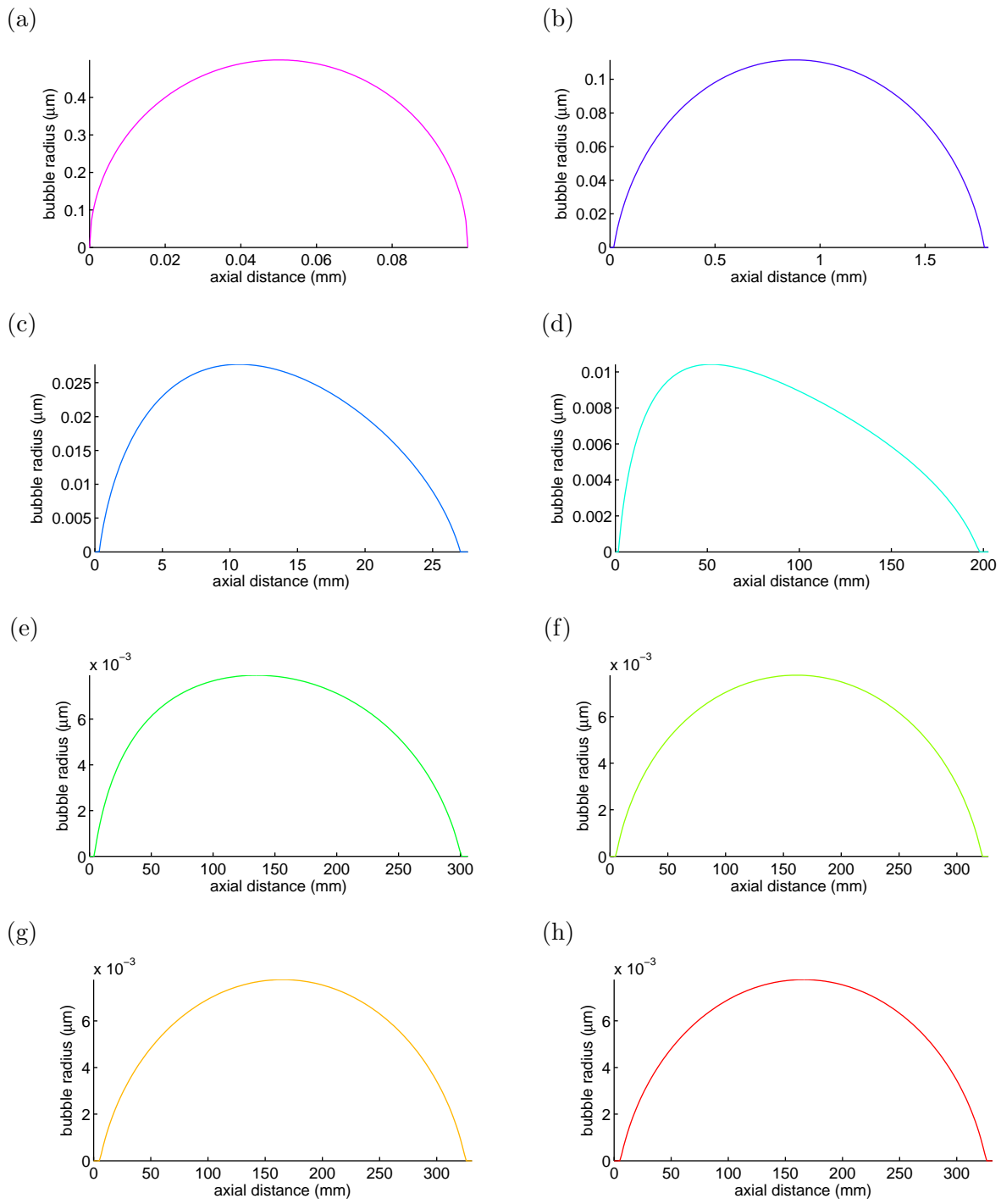
14

Figure 5: Evolution of a convex bubble. Left-end positions at (a) 0.4 m, (b) 0.5 m, (c) 0.6 m, (d) 0.7 m, (e) 0.8 m, (f) 0.9 m, (g) 1.0 m and (h) 1.1 m. Axial distance is given relative to the left-end positions.
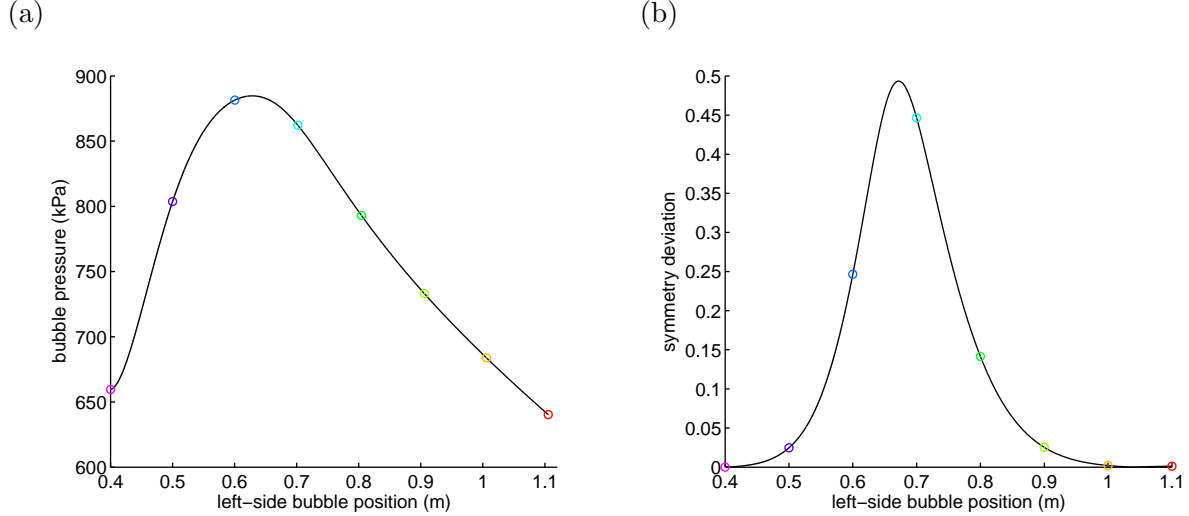
(a)

(b)

Figure 6: (a) Bubble pressure and (b) L_2 deviation from symmetry about the midpoint of the bubble. Color marks correspond to bubble shapes given in Figure 5.

The initial bubble shape has fore-aft symmetry, and the two bubbles that appear in the final plot appear to be mirror images of one another. However, the two bubbles are not quite symmetric. The left bubble has an axial distance of 0.1531 m and a maximum radius of 7.887×10^{-9} m while the right bubble has an axial distance of 0.1532 m and a maximum radius of 7.893×10^{-9} m. The pressure for each bubble is also different as may be seen in the plots of pressure in Figure 8. In this figure, we note that the pressure for the left bubble after pinch-off is generally larger than that for the right bubble.

4   Leaky-mass model

In this section, we consider an extension of the model considered previously in which the mass of the gas in the bubble is allowed to diffuse into the surrounding glass. The governing equations for the glass are unchanged in this "leaky-mass" model, but the equations for the bubble are modified to take into account mass flow into or out of the bubble. The first part of the section describes the governing equations of the model, while the second part discusses a suggested numerical method of solution of the equations.

4.1   Governing equations

The first step in the derivation of the extended model is to obtain an equation governing mass diffusion in the glass surrounding the bubble. Let $C(r, z, t)$ be the mass concentration of gas in the glass at a radial position r, axial position z and time t. In the vicinity of the bubble $r = h(z, t)$ we assume that C solves the convection-diffusion equation

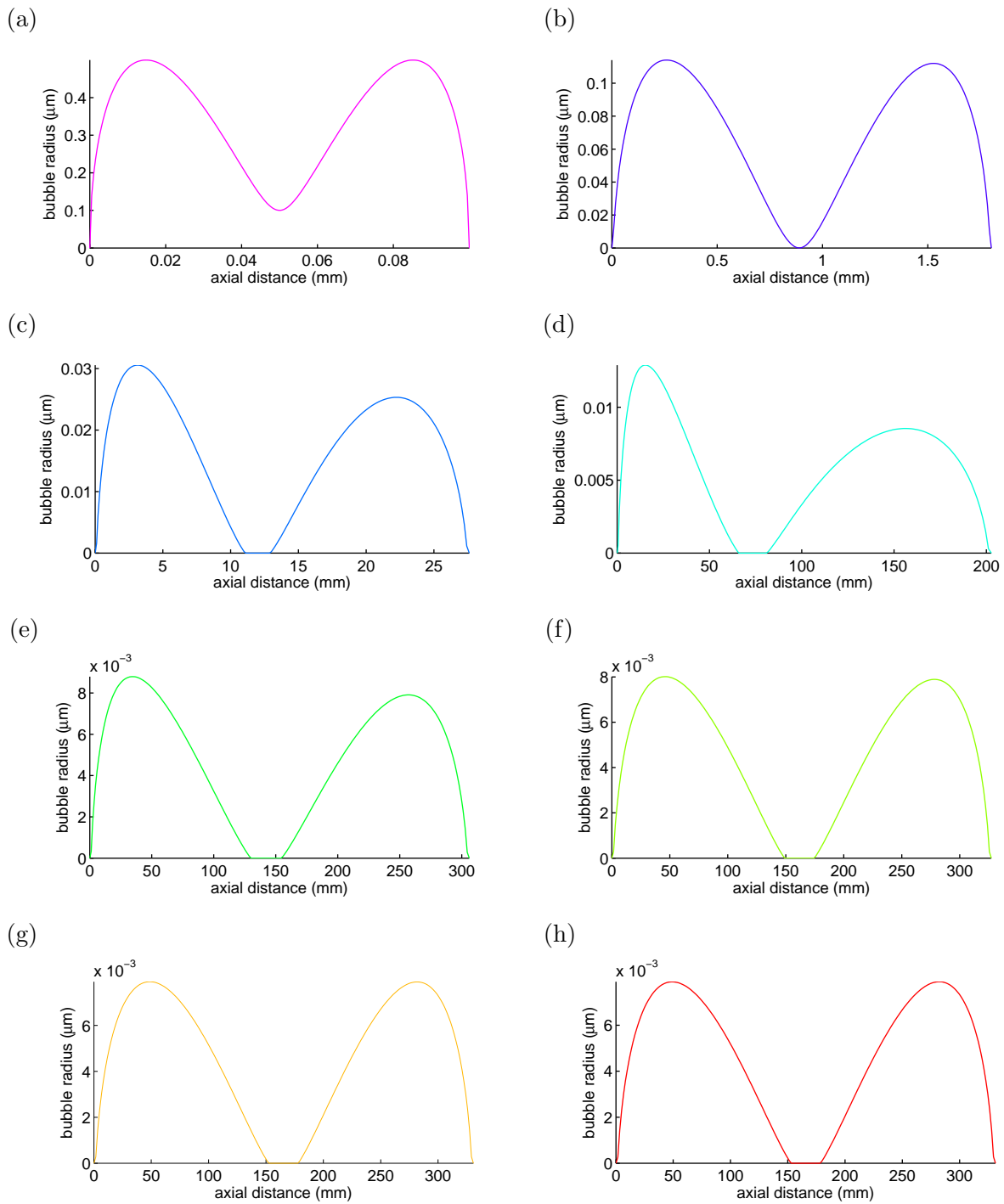$$(rC)_t + (rwC)_z + (ruC)_r = (DrC_r)_r, \tag{28}$$

16

Figure 7: Evolution of a non-convex bubble. Left-end positions at (a) 0.4 m, (b) 0.5 m, (c) 0.6 m, (d) 0.7 m, (e) 0.8 m, (f) 0.9 m, (g) 1.0 m and (h) 1.1 m. Axial distance is given relative to the left-end positions.
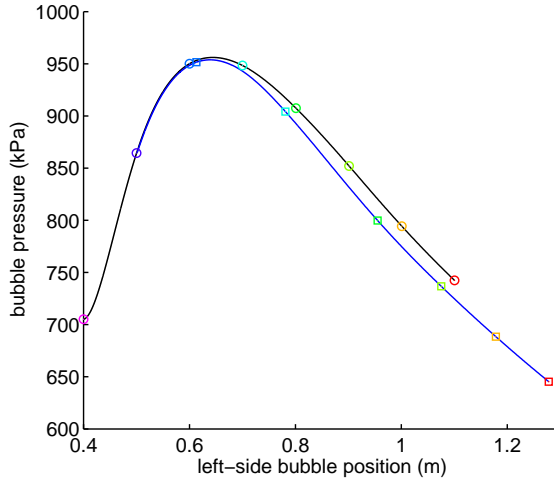
17

Figure 8: Bubble pressure for a non-convex bubble shape. The black curve corresponds to the bubble pressure prior to pinch-off and to the left-most bubble after pinch-off, while the blue curve corresponds to the pressure of the right-most bubble after pinch-off. Color marks correspond to bubble shapes given in Figure 7.

where (u, w) is the velocity of the glass and $D = D(T)$ is the diffusion coefficient (which depends on the glass temperature). According to Fitt *et al.* [1], we have

$$ru = -\frac{r^2}{2} w_z + \frac{1}{2\mu} \left(Pq - \gamma \sqrt{q} \right), \qquad q = h^2.$$

As before, we consider the change of variables $(r, z, t) \to (\hat{r}, x, \hat{t})$, where

$$\hat{r} = r, \qquad x = \int_{z_0}^{z} \frac{A(\zeta)}{A_0} \, d\zeta, \qquad \hat{t} = t,$$

so that

$$\frac{\partial}{\partial r} = \frac{\partial}{\partial \hat{r}}, \qquad \frac{\partial}{\partial z} = \frac{A}{A_0} \frac{\partial}{\partial x} = \frac{w_0}{w} \frac{\partial}{\partial x}, \qquad \frac{\partial}{\partial t} = \frac{\partial}{\partial \hat{t}}.$$

In terms of the new variables, (28) becomes (without hats)

$$C_t + \frac{w_0}{w} \left(wC \right)_x + \frac{1}{r} \left(ruC \right)_r = \frac{D}{r} \left(rC_r \right)_r, \tag{29}$$

where

$$ru = -\frac{r^2}{2} \frac{w_0}{w} w_x + \frac{1}{2\mu} \left(Pq - \gamma \sqrt{q} \right). \tag{30}$$

Using (30) in (29) gives

$$C_t + w_0 C_x + uC_r = \frac{D}{r} \left(rC_r \right)_r, \qquad u = -\frac{r}{2} \frac{w_0}{w} w_x + \frac{1}{2r\mu} \left(Pq - \gamma \sqrt{q} \right). \tag{31}$$

18

For later purposes, it is convenient to consider the change of variables $(r, x, t) \rightarrow (\eta, \hat{x}, \hat{t})$, where

$$\eta = \frac{r}{h(x, t)}, \qquad \hat{x} = x, \qquad \hat{t} = t,$$

so that

$$\frac{\partial}{\partial r} = \frac{1}{h} \frac{\partial}{\partial \eta}, \qquad \frac{\partial}{\partial x} = \frac{\partial}{\partial \hat{x}} - \eta \frac{h_x}{h} \frac{\partial}{\partial \eta}, \qquad \frac{\partial}{\partial t} = \frac{\partial}{\partial \hat{t}} - \eta \frac{h_t}{h} \frac{\partial}{\partial \eta}.$$

In terms of the new variables, the equations in (31) become (without hats)

$$C_t + w_0 C_x - \eta \left(\frac{h_t + w_0 h_x}{h} \right) C_\eta + \frac{u}{h} C_\eta = \frac{D}{\eta h^2} (\eta C_\eta)_\eta, \qquad u = -\frac{\eta h}{2} \frac{w_0}{w} w_x + \frac{1}{2\eta h \mu} (Pq - \gamma \sqrt{q}). \tag{32}$$

Recall that $y = wq = wh^2$ so that

$$\frac{h_t + w_0 h_x}{h} = \frac{q_t + w_0 q_x}{2q} = \frac{y_t + w_0 y_x}{2wq} - \frac{w_0}{2w} w_x.$$

Then, using the bubble equation in (19), we have

$$\frac{h_t + w_0 h_x}{h} = \frac{1}{2q\mu} (Pq - \gamma \sqrt{q}) - \frac{w_0}{2w} w_x. \tag{33}$$

So, using (33) the equations in (32) reduce to

$$C_t + w_0 C_x - \frac{Pq - \gamma \sqrt{q}}{2\mu q} \left(\eta - \frac{1}{\eta} \right) C_\eta = \frac{D}{\eta q} (\eta C_\eta)_\eta.$$

Finally, we can switch to (η, ξ, t), where $\xi = x - w_0 t$, to get

$$C_t - \frac{Pq - \gamma \sqrt{q}}{2\mu q} \left(\eta - \frac{1}{\eta} \right) C_\eta = \frac{D}{\eta q} (\eta C_\eta)_\eta, \qquad \eta > 1, \quad \xi_\ell < \xi < \xi_r, \quad t > 0. \tag{34}$$

The initial condition for the convection-diffusion equation in (34) is

$$C(\eta, \xi, 0) = C_0, \qquad \text{for } \eta > 1 \text{ and } \xi_\ell < \xi < \xi_r,$$

where C_0 is an equilibrium concentration of gas in the glass. The boundary conditions are

$$C(1, \xi, t) = \Lambda \rho_g(\xi, t) = \Lambda \left[\frac{P(t) + P_a}{R_m T(z(\xi + w_0 t))} \right], \qquad \text{for } \xi_\ell < \xi < \xi_r \text{ and } t > 0 \tag{35}$$

where Λ is a saturation constant, and

$$C = C_0, \qquad \text{as } \eta \rightarrow \infty \text{ for } \xi_\ell < \xi < \xi_r \text{ and } t > 0 \tag{36}$$

Having derived a PDE for the mass concentration of gas along with initial conditions and boundary conditions, the next step in the description of the extended model is to link the behavior of C to that of the bubble. The shape of the bubble determined by $y(\xi, t)$ solves (21) as before, but

the pressure $P(t)$ in the equation is no longer described by the fixed-mass integral in (22). Instead, the now time-dependent mass of the gas in the bubble is given by

$$\mathcal{M}_g(t) = \frac{\pi \left(P(t) + P_a\right)}{w_0 R_m} \int_{\xi_\ell}^{\xi_r} \frac{y(\xi, t)}{T(z(\xi + w_0 t))} \, d\xi. \tag{37}$$

The evolution of the mass is determined by the flux of gas into or out of the glass, i.e.

$$\frac{d}{dt}\mathcal{M}_g(t) = -\int_{\mathcal{S}_b} \left(\mathbf{J}_b \cdot \mathbf{n}_b\right) dS,$$

where $\mathcal{S}_b$ is the surface area of the bubble, $\mathbf{J}_b = -D\nabla C|_{\mathcal{S}_b}$ is the flux of gas into the glass at the bubble surface, and $\mathbf{n}_b$ is the unit outward normal on the surface of the bubble. Assuming that $|h_z| \ll 1$, we find

$$\frac{d}{dt}\mathcal{M}_g(t) = 2\pi A_0 \int_{\xi_\ell}^{\xi_r} \frac{D(T(z(\xi + w_0 t))) \, C_\eta(1, \xi, t)}{A(\xi + w_0 t)} \, d\xi \,. \tag{38}$$

The initial condition for (38) is that $\mathcal{M}_g(0)$ is given, and then (37) may be applied at $t = 0$ to determine $P(0)$. This completes the description of the governing equations for the leaky-mass model.

4.2 Suggested numerical approach

The governing equations for the leaky-mass model are given by (21), (34), (37) and (38) for the unknowns $y(\xi, t)$, $C(\eta, \xi, t)$, $P(t)$ and $\mathcal{M}_g(t)$. As before, the equations require a known temperature distribution given by $T(z)$. The equations also require the area $A(z)$ and axial velocity $w(z)$ of the glass fiber as input, and these two quantities can be determined from a numerical integration of (17) and (18) as described previously in Section 3.3. The purpose of the present discussion is to outline a numerical approach which may be used to determine the remaining four quantities of the model.

The simplest numerical approach would involve an explicit time integration of the equations. Let us assume that y, C, P and $\mathcal{M}_g$ are known at a time t on a uniform grid

$$\xi_j = \xi_\ell + j\Delta\xi, \qquad j = 0, 1, \ldots, N, \qquad \Delta\xi = (\xi_r - \xi_\ell)/N,$$

and

$$\eta_k = 1 + k\Delta\eta, \qquad k = 0, 1, \ldots, K, \qquad \Delta\eta = (\eta_\infty - 1)/K,$$

where N and K are chosen positive integers and η_∞ is taken to be large. Standard centered finite differences may be used to approximate the η-derivatives in (34) and (38) so that (21), (34) and (38) become ODEs for $y(\xi_j, t)$, $C(\eta_k, \xi_j, t)$ and $\mathcal{M}_g(t)$. An explicit time-integration of these three equations would give y, C and $\mathcal{M}_g$ at a time $t + \Delta t$. The integral equation in (37) could then be evaluated numerically to obtain P at $t + \Delta t$, which completes the time step. The time-stepping procedure would begin by applying initial conditions to all four of the variables, and then the time integration step would be repeated iteratively until a chosen time is reached corresponding to the time needed for the bubble to travel the axial distance of the drawing tower.

20

5 Conclusions

Mathematical models that describe the dynamical behavior of a thin gas bubble embedded in a glass fiber during a fiber drawing process have been discussed and analyzed. The aim of the analysis was to address the questions posed by the representative from Corning, which were listed previously in Section 1. The starting point for the mathematical modeling was the equations presented in [1] for a glass fiber with a hole undergoing extensional flow. These equations were reconsidered here with the additional reduction that the hole, i.e. the gas bubble, was thin as compared to the radius of the fiber and of finite extent. The primary model considered was one in which the mass of the gas inside the bubble was fixed. This *fixed-mass* model involved equations for the axial velocity and fiber radius, and equations for the radius of the bubble and the gas pressure inside the bubble. The model equations assumed that the temperature of the furnace of the drawing tower was known, and this input was provided by Corning.

The governing equations of the bubble are hyperbolic and predict that the bubble cannot extend beyond the limiting characteristics specified by the ends of the initial bubble shape. An analysis of pinch-off was performed, and it was found that pinch-off can occur, depending the parameters of the model, due to surface tension when the bubble radius is small. In order to determine the evolution of a bubble, a numerical method of solution was presented. The method was used to study the evolution of two different initial bubble shapes, one convex and the other non-convex. Both initial bubble shapes had fore-aft symmetry, and it was found that the bubbles stretched and elongated severely during the drawing process. For the convex shape, fore-aft symmetry was lost in the middle of the drawing process, but the symmetry was re-gained by the end of the drawing tower. A small amount of pinch-off was observed at each end for this case, so that the final bubble length was slightly shorter than its theoretical maximum length. For the non-convex initial shape, pinch-off occurred in the middle of the bubble resulting in two bubbles by the end of the fiber draw. The two bubbles had different final pressures and did not have fore-aft symmetry. We recognize that a further numerical investigation is needed to investigate other possible phenomena under different drawing conditions and with different parameter values.

An extension of the fixed-mass model was considered in which the gas in the bubble was allowed to diffuse into the surrounding glass. The governing equations for this leaky-mass model were developed and manipulated into a form suitable for a numerical treatment. A numerical method of solution was suggested but no numerical solutions were found. This is an aspect of the problem that may be considered in future work.

References

[1] A. D. Fitt, K. Furusawa, T. M. Monro, C. P. Please, D. J. Richardson, The mathematical modelling of capillary drawing for holey fibre manufacture, J. Eng. Math. 43 (2002) 201–227.

[2] C. J. Voyce, A. D. Fitt, T. M. Monro, The mathematical modelling of rotating capillary tubes for holey-fibre manufacture., J. Eng. Math. 60 (2008) 69–87.

[3] M. A. Matovich, J. R. A. Pearson, Spinning a molten threadline – Steady-state isothermal viscous flows, Ind. Eng. Chem. Fundam. 8 (1969) 512–520.

[4] J. R. A. Pearson, M. A. Matovich, Spinning a molten threadline – Stability, Ind. Eng. Chem. Fundam. 8 (1969) 605–609.

[5] Y. T. Shah, J. R. A. Pearson, On the stability of non-isothermal fiber-spinning, Ind. Eng. Chem. Fundam. 11 (1972) 145–149.

[6] Y. T. Shah, J. R. A. Pearson, On the stability of non-isothermal fiber-spinning – general case, Ind. Eng. Chem. Fundam. 11 (1972) 150–153.

[7] J. A. Bergman, Liquid glass jets in the forming of continuous fibers, Glass Technol. 11 (1970) 110–116.

[8] L. R. Glicksmann, The cooling of optical fibers, Glass Technol. 9 (1968) 131–138.

[9] G. Manfre, Forces acting in the continuous drawing of glass fibres, Glass Technol. 10 (1969) 99–106.

[10] M. M. Denn, Continuous drawing of liquids to form fibers, Ann. Rev. Fluid Mech. 12 (1980) 365–387.

[11] C. J. S. Petrie, One hundred years of extensional flow, J. Non-Newtonian Fluid Mech. 137 (2006) 1–14.

[12] J. Dewynne, J. R. Ockendon, P. Wilmott, On a mathematical model for fiber tapering, SIAM J. Appl. Math. 49 (1989) 983–990.

[13] J. Dewynne, P. D. Howell, P. Wilmott, Slender viscous fibres with inertia and gravity, Q.J. Mech. Appl. Math. 47 (1994) 541–555.

[14] P. D. Howell, Extensional thin-layer flows, Ph.D. thesis, University of Oxford (1994).

[15] L. J. Cummings, P. D. Howell, On the evolution of non-axisymmetric viscous fibres with surface tension, inertia and gravity, J. Fluid Mech. 389 (1999) 361–389.

[16] P. D. Howell, J. J. Wylie, H. X. Huang, R. M. Miura, Stretching fo heated threads with temperature-dependent viscosity: Asymptotic anaysis, Discrete and Continuous Dynamical Systems 7.

[17] J. J. Wylie, H. Huang, Extensional flows with viscous heating, J. Fluid Mech. 571 (2007) 359–370.

[18] C. J. Voyce, A. D. Fitt, T. M. Monro, Mathematical modeling as an accurate predictive tool in capillary and microstructured fiber manufacture: The effects of preform rotation., J. Lightwave Tech. 26 (2008) 791–798.

[19] H. X. Huang, J. J. Wylie, R. M. Miura, P. D. Howell, On the formation of glass microelectrodes, SIAM J. Appl. Math. 67 (2006) 630–666.

[20] I. M. Griffiths, P. D. Howell, The surface-tension driven evolution of a two-dimensional annular viscous tube, J. Fluid Mech. 593 (2007) 181–206.

[21] I. M. Griffiths, P. D. Howell, Mathematical modelling of non-axisymmetric capillary tube drawing, J. Fluid Mech. 605 (2008) 181–206.

[22] I. M. Griffiths, Mathematical modelling of non-axisymmetric glass tube manufacture, Ph.D. thesis, University of Oxford (2008).

[23] C. J. Voyce, A. D. Fitt, T. M. Monro, Mathematical model of the spinning of microstructured optical fibres, Optics Express 12 (2004) 5810–5820.

[24] P. D. Howell, M. Siegel, The evolution of a slender non-axisymmetric drop in an extensional flow, J. Fluid Mech. 521 (2004) 155–180.